Development of coated, annular fins for adsorption chillers

S.D. Waszkiewicz, M.J. Tierney, H. Saidani Scott

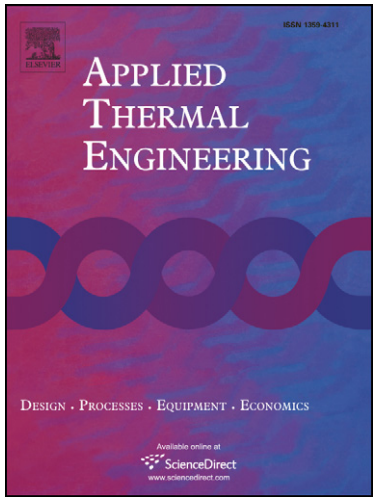

Development of coated, annular fins for adsorption chillers

S.D. Waszkiewicz, M.J. Tierney, H. Saidani Scott

PII: S1359-4311(08)00451-1
DOI: 10.1016/j.applthermaleng.2008.11.004
Reference: ATE 2656

To appear in: *Applied Thermal Engineering*

Received Date: 4 March 2008
Revised Date: 24 July 2008
Accepted Date: 6 November 2008

Please cite this article as: S.D. Waszkiewicz, M.J. Tierney, H.S. Scott, Development of coated, annular fins for adsorption chillers, *Applied Thermal Engineering* (2008), doi: 10.1016/j.applthermaleng.2008.11.004

DEVELOPMENT OF COATED, ANNULAR FINS FOR ADSORPTION CHILLERS

S. D. Waszkiewicz British Energy, Gloucestershire, UK

M. J. Tierney* Department of Mechanical Engineering, University of Bristol, UK

H. Saidani Scott Department of Mechanical Engineering, University of Bristol, UK

* corresponding author.

ABSTRACT

The specific cooling power (SCP) of adsorption chillers could be increased by employing zeolite coated, extended heat transfer surfaces in the generator. An experiment featured 50 annular aluminium fins, 76 mm diameter, each coated with 2 grams of zeolite CBV901, and pressed onto a 10 mm bore aluminium tube. A large (4 kg), structurally stiff and easily fabricated casing enclosed the finned tube; the resulting generator assembly formed a “thermal compressor”, increasing the pressure

of methanol vapour from ~100 to ~280 kPa. During a typical thermal cycle the peak-to-peak temperature changes were: casing temperature 35 K; methanol vapour (inside the generator) 45K; the fin 65K; heat transfer liquid 80K. On a Clapeyron diagram, a non-ideal, anisosteric depressurisation stage was attributed to the relatively high mass of refrigerant vapour in the generator (~1 g, compared with at least ~8g held in the zeolite). The radial temperature profile along the fin was modelled by lumping the energy contents of the aluminium and the bonded zeolite into an effective heat capacity. Thereupon, the model was fitted to recorded data - the adjustable coefficiencts inside the model related to the thermal resistance of the tube-to-fin-root interface. The best-fit incurred a root mean square error of 3.5 K, at which point the interfacial resistance governed heat transfer and hence cooling power. Based on computed heat transfer to the fin, the inferred coefficient of performance was 41%; this could be improved by eliminating the interfacial resistance and optimising the fin thickness.

Keywords: adsorption chillers; coated surfaces; heat transfer

NOMENCLATURE

c	specific heat capacity (kJ kg^{-1} K^{-1})
e	root mean square discrepancy (Eq. 6) (K)
h	heat transfer coefficient (kW m^{-2} K^{-1})
H	enthalpy of adsorption (kJ kg^{-1})
k	constant in Dubinin Astakahov equation (-)
m	mass (kg)
Nu	Nusselt number (-)
n	constant in Dubinin Astakahov equation (-)
r	radial distance (m)
R	tube radius (m)
t	time (s)
T	temperature (measured) (K)
w	fin thickness (m)
X	adsorption capacity (-)
X_o	constant in Dubinin Astakahov equation (-)
Y	temperature (predicted) (K)

Greek symbols

α	constant term (Eq. 5) (kW m^{-2} K^{-1})
β	constant term (Eq. 5) (kW m^{-2} K^{-2})
λ	thermal conductivity (kW m^{-1} K^{-1})

ρ	density (aluminium) (kg m^{-3})

Subscripts

al	aluminium
ar	refrigerant in adsorbed phase
i	inner surface of tube
l	lower flank
iface	tube-to-fin interface
liq	heat transfer fluid
o	outer surface of tube
s	saturation value
u	upper flank
v	vapour
z	zeolite
+	fin-side of interface

INTRODUCTION

This paper concerns the likely performance of compact adsorption refrigerators driven by low-grade heat. In Europe, Japan and Northern America, for example, refrigeration and air conditioning consumes 15% to 20% of the primary energy diverted to buildings [1] [2]. Consequently, technologists are motivated to develop [3] and manufacture [4] chillers that exploit waste streams with low specific exergy (for instance, waste heat from fuel cells).

Absorption machines are presently the most commonly manufactured form of heat-operated refrigeration. LiBr-water pairs exploit heat supplies at between 70°C and 160°C [5] but replacing water cooling with air cooling is often impractical because the higher absorber temperatures would ultimately force larger mass fractions of LiBr and a greater risk of crystallisation [6]. Pumping corrosive liquid is a further problem.

Adsorption units can be air-cooled, and have been demonstrated successfully over the last ten to fifteen years [7]. Ranked in ascending order of operating pressures, the preferred refrigerants are water, methanol, or ammonia. Unfortunately slow heat transfer to and from the solid adsorbent bed tends to make the specific cooling power (SCP) many times less than that expected for vapour compression cycles; for example in a basic zeolite-water system the measured SCP was 25 W (maximum) per kg of zeolite [8]. For the purposes of this paper, our aim has been to investigate the potential of coated surfaces to improve heat transfer, in complete adsorption cycles.

Specifically, the substrate was aluminium, the adsorbent-refrigerant pair was zeolite CBV901-methanol and coated annular fins extended the available heat transfer area.

Several workers have coated solid adsorbents directly onto tubular heat transfer surfaces, rather than using a packed bed, so as to improve heat transfer. Few papers relate to the use of such surfaces in complete cycles, or to the use of extended surfaces. The hydrothermal crystallisation of zeolite layers is time consuming; for instance a three-to-five-hour-long process is needed to increase the layer thickness by 3 μm; successive coatings have produced 2mm-thick layers [9] [10] . The thermal conductivity of the layer is four times that of a bed packed with the same material, and the surface-to-layer heat transfer coefficient is 3000 W m^{-2} K^{-1} versus 25 W m^{-2} K^{-1} for a packed bed. Simulation indicates a potential four-fold improvement in specific cooling power (SCP) [9]. Waszkiewicz et al. [11] bonded layers of zeolite CBV901 to an aluminium substrate with cellulose methyl ether (commonly known as wallpaper paste). Although layers thicker than 2mm cracked, the mechanical properties appeared no worse than those of the published alternatives, and far less labour was needed. The adsorptive capacity was satisfactory (up to 29% at 30°C).

This paper describes an experiment to study the performance of a coated finned tube. After the methods section, histories of temperature and pressure vs. time are presented. We describe methods of fitting measured fin-tip temperatures to mathematical models, and thereby identify the rate determing step for this experiment (the thermal resistance of the interface between the tube and the fin).

EXPERIMENTAL METHODS

The generator formed the most important experimental feature (Fig. 1, part 1). It was cooled and heated via the same finned pipe (10 mm bore), fed from hot/ cold reservoirs (each 105 litres in volume). The heat transfer liquid was either water or Transcal N mineral oil. Each of the 50 annular fins was manufactured from aluminium, measured 76mm outer diameter, 12.5 mm inner diameter and 2 mm thickness, and the fin spacing was 125 mm. The coating on each fin surface contained 1.0 g of powdered zeolite CBV901 particles, 15.9 μm in Sauter mean diameter. (Particle diameters were measured with a Malvern 2600 series diffraction based particle sizer). The coating procedure was (1) degrease the fin surface with acetone (2) etch by immersion in chromic acid at 60^{o}C for 30 minutes (3) adhere with a mixture of 10% w/w cellulose methyl ether and 90% w/w zeolite powder (4) dry for 12 hours at 120°C. After coating the fins were press fitted onto an aluminium heating/ cooling tube (10 mm bore, 12.5 mm outer diameter).

The generator was oriented vertically to give direct access to the evaporator. A reviewer has since correctly pointed out that a horizontal mounting might well have modified heat and mass transfer to the fins

The adsorption capacity of a single fin was measured volumetrically (sample volume of 1 litre, full details in [11] and [12]). The measurements were close to Tchernev's

data fit for the same pair [13] (Fig. 2, part a). A least squares procedure fitted adsorption capacities to the Dubinin Astakanov equation. [14] (Fig. 2, part b)

$$X = X_o\left[k\left(\frac{T}{T_s}-1\right)^n\right] \quad (1)$$

where the constants are X_0 =0.218 , k = -28.4788, n=1.7 and T_s is the saturation temperature.

The aluminium generator was mechanically robust, at the cost of a relatively large heat capacity of 3.0 kJ K^{-1} and a relatively large volume of 4.34 l. Vacuum fittings, containing nitrile o-rings and sealed with vacuum grease, were used throughout the rig. The valves were manually operated.

Temperatures, pressures, and rates of condensation were recorded. Thermocouples were fabricated by the spot-welding of K-type, 0.2mm diameter wires onto the inner surfaces of the generator at several locations (Fig. 3). Checks demonstrated that similar thermocouples, formed on aluminium coupons, were consistent with mercury thermometers to ± 1K. Stainless-steel sheathed thermocouples were attached to the hot/ cold reservoirs. Probes were monitored at 10 s intervals. Generator pressure was monitored with an Edwards ASG-NW16 gauge (quoted accuracy 0.2% of the full scale deflection of 100 kPa). As regards the calibrated receiver (below the condenser), we consider the 1 ml graduations to correspond to a fair error estimate.

To establish the leak-tightness of the experiment, all gas was evacuated through a helium detector; helium was released near joints to locate any specific leaks. Thereafter the rig was sealed under near total vacuum and its pressure monitored versus time; a pressure rise limited to 7 kPa within six hours was achievable, versus minimum refrigerant pressures of 80 kPa under operation.

RECORDED TEMPERATURES AND PRESSURES

This paper reports temperatures and pressures from one out of four completed runs. The heat capacity of the shell damped the fluctuations in vapour temperature, ensuring that the vapour was always either substantially hotter or substantially colder than the fin. Fig. 4 shows temperatures of the heat transfer fluid (T7), the fin tip (T5), and the refrigerant vapour (T3). Temperatures variations in the generator casing were generally small (T12, T13), except for those parts closer to the heat transfer pipe (T14).

Fig. 5 shows evaporator and generator pressure plotted against time. Note that the generator was slightly underpressurised at the start of an evaporation step (roughly 8000 s), attributable to late (manual) valve operation. A Clapeyron diagram (Fig. 6) plots the fin temperature versus the generator pressure. This result was different to the idealised cycle, particularly during depressurisation. The principle non-ideality was the relatively high mass of vapour in the generator – by calculation 1 g vapour phase compared with 8 g adsorbed phase at the start of depressurisation - so that the generator was depressurised anisosterically. A further non-ideality was the temperature gradient in the fin - the next section will suggest a small difference of ±2

K from root to tip. The computed changes in loading agreed with the measured condensation rate to within ±15%.

DATA ANALYSIS

The recorded temperatures were data-fitted. The model assumed (1) no azimuthal or vertical variation in the temperature of the coated fin (2) mass transfer within the coating influenced the temperature development far less than heat transfer to the fin (see, for example, reference [15]). The second assumption is fair for longer cycle times, far exceeding the characteristic time of typically two minutes for diffusion into the zeolite layer.

For radial, time dependent conduction in an annular fin,

$$\rho c_f \frac{\partial T}{\partial t} = \frac{1}{r}\frac{\partial}{\partial r}\left(r \lambda \frac{\partial T}{\partial r} \right) + \left(\frac{h_u + h_l}{w} \right)\left(T_v - T \right) \qquad (2)$$

where h_u and h_l are the heat transfer coefficients from the upper and lower flanks respectively of the fin to the vapour refrigerant, T is the fin temperature, λ is the thermal conductivity of aluminium, and, importantly, c_f is an effective heat capacity, lumping heat storage in the fin and the bonded zeolite. Terms such as d/dt were found with the first order accurate Euler method (time step = 0.1s) and a special form [16] of Orthogonal Collocation [17] yielded the radial gradients. It had been tested with four and six internal points and was consistently accurate to 0.5% when compared to reduced analytic solutions for heat flux.

Term c_f (in Equation 2) is a lumped heat capacity,

$$c_f = c_{al} + \frac{m_z}{m_{al}}\left(c_z + X c_{ar} - \delta(t) H \frac{\partial X}{\partial T} \right) \tag{3}$$

where m_z is the mass of the zeolite part of the fin, $\delta(t) = 0$ for isosteric pressurisation and $\delta(t) = 1$ for isobaric desorption, and H is the enthalpy of adsorption, inferred from the enthalpy of vaporisation by Van't Hoff arguments. For flanks hotter than the surrounding vapour, the estimated heat transfer coefficients were [18],

$$Nu = \begin{cases} 0.54\,Ra^{0.25} & ,\left(2x10^4 < Ra < 10^7,\ upper\ \ flank\right) \\ 0.27\,Ra^{0.25} & ,(10^5 < Ra < 10^{11},\ lower\ \ flank) \end{cases} \tag{4}$$

where the Nusselt number (Nu) and Rayleigh number (Ra) are based on the fin diameter and local flank-to-vapour temperature difference. (The discussion section deals with imperfections in these correlations) The tip of the fin was treated as adiabatic, and conjugate heat transfer held at the fin root,

$$\frac{1}{\frac{R_o}{R_i}\frac{1}{h_i} + \frac{1}{h_{iface}}}\left(T_{liq} - T\left(R_{o,+}\right)\right) = -\lambda \left.\frac{\partial T}{\partial r}\right|_{r=R_{o,+}} \tag{5}$$

where + signifies the fin side of the tube-to-fin interface. Term h_i, the heat transfer coefficient on the inner surface of the tube, was estimated conservatively as 6.4 kW m^{-2} K^{-1} with the Dittus-Boelter equation, after checks using an open circuit, container and stopwatch, demonstrated average water velocities in excess of 1 m s^{-1}. The interfacial conductance from tube to fin was modelled as an arbitary function of the liquid-to-fin temperature difference,

$$h_{iface} = \alpha + \beta\left(T_{liq} - T\left(R_{o,+}\right)\right) \quad (6)$$

(Arguably, the interfacial forces due to thermal expansion were proportional to the applied temperature difference, and it is reasonable to estimate the interfacial conductance as varying in proportion to the interfacial force and thus the temperature difference)

The analysis treated a single desorption stage. Fig. 7 presents measured and predicted temperatures at the fin tip, for which parameters α and β are located at the minimum on Fig. 8, a contour plot of root mean square (r.m.s.) error, e. A total of 120 trial calculations were completed, each with its own values of (α, β), and producing a r.m.s. error according to,

$$e = \sqrt{\frac{\sum_N \left(Y_i^2 - T_i^2\right)}{N}} \quad (7)$$

where Y is predicted fin temperature, T is the measured value, and N is the number of measurements.

DISCUSSION

For Fig. 7, the predicted interfacial conductances were initially h_{iface} = 1.5 kW m^{-2} K^{-1} decreasing to 0.8 kW m^{-2} K^{-1}, and less than the tube side heat transfer coefficient (h_i = 6.4 kW m^{-2} K^{-1}). This conclusion held true for a range of estimated heat transfer coefficients at the flanks. Arguably, the blockage caused by adjacent fins might have reduced the flank heat transfer coefficients. Calculations were repeated by halving the

estimated heat transfer coefficients from Equation 4 (that is $h = 0.5\ h_{correlation}$); there was practically no shift in the location of the minimum on Fig. 8 (β was reduced by 0.1 W m^{-2} K^{-2}) and hence no change in the interfacial conductances. In the first 500 seconds of operation the Rayleigh number was below the lower limits in Equation 4 ($Ra = 8.8 \times 10^4$ at a flank-to-vapour temperature difference of 20 K), so that h_l might have been underestimated slightly; Eqn. 4 incorrectly implies $Nu \rightarrow 0$ as $Ra \rightarrow 0$. Repeating calculations with $h = 2\ h_{correlation}$ led to h_{iface} in the range 1.9 to 0.8 kW m^{-2} K^{-1} - still less than h_i.

The relatively low interfacial conductance would justify extruding fins from the base material [19] so as to eliminate the interface and improve heat transfer and ultimately SCP ($h_{iface} \rightarrow \infty$ in Equation 4). Alternatively the inner tube could be expanded; fins could then be coated separately before assembly.

The liquid film on the tube-side forces two trade-offs. (1) Larger tube diameters would provide a larger heat transfer boundary with the fin, but the heat capacity of inert material in the tube would be greater. (2) The value of h_i would increase if the liquid flow rate were increased, but at the cost of more pumping power.

From calculation (Equations 2 to 5 and Fig. 7), the heat transmitted to fins was 4.0 kJ per fin per cycle, compared with a refrigeration effect of 1.7 kJ per fin per cycle and fin-to-vapour heat transfer of 0.20 kJ per fin per cycle. (One the basis of the surface area of the flanks, these values become 56 W m^{-2}, 24 W m^{-2} and 3 W m^{-2} respectively). Ignoring the very large losses from thermally cycling the generator casing (and the tube), the coefficient of performance based on fins in isolation was

1.7÷4.0 = 42%, and the specific cooling power was 10 W per kg of coated fin or 40 W per kg of adsorbent. If machines could be fabricated with the thermal mass of the casing and tubes substantially less than that of the fins, then the performance would compete with current commercial machines [4]. Also from calculations, the temperature difference from fin root to fin tip was 2K at most. In principle thinner fins might have been used, reducing the heat capacity of inert material.

The model fitted fin temperatures better when the vapour side heat transfer coefficient, h, was treated as a parameter (1K error only). However, the conclusion about the importance of the interface was the same, the best fit corresponded to an unphysical value of h =20 W m^{-2} K^{-1}(compared with a maximum of 4.8 W $m^{-2}K^{-1}$ for the upper flank, Equation 4), and the detailed analysis does not warrant reporting here. A better fit might in future be achieved with a model of mass transfer; this would necessitate more detailed measurements of inter- and intra particle mass diffusivities.

CONCLUSIONS

An experiment is available to test the performance of zeolite-coated annular fins over complete adsorption cycles. The coating process was less laborious than previously reported. The temperature and pressure histories in the generator indicated large heat losses to the generator casing. A model of heat transfer could be fitted to recorded temperatures adequately (4.0 K r.m.s. error). It indicated that the fin-to-tube interface controlled SCP.

ACKNOWLEDGEMENT

We thank the government of the United Kingdom for supporting Dr Waskiewicz under the ORS scheme.

REFERENCES

1. D. McFarland, Energy, efficiency, and the environment. 6th Gustav Lorentzen natural working fluids conference, University of Glasgow, UK 2004.

2. European Commission Directorate-General for Energy and Transport, Europa. EU-15 european energy and transport trends to 2030. (2003).

3. F. Meunier, Solid sorption: An alternative to CFCs. Heat recovery systems and CHP 13(4), (1993), 289-295.

4. MyCom (Canada), Technical brochure. www.mycomcanada.com/Brochure/adref series.pdf

5. W. F. Stoeker and J. W. Jones, Refrigeration and air conditioning. 2nd Ed., McGraw Hill International, New York, 1982.

6. J. Yoon and O. Kwon, Cycle analysis of air-cooled adsorption chiller using a new working solution. Energy 24(9), (1999), 795-809.

7. R. Critoph and Y. Zhong, Review of trends in solid sorption refrigeration and heat pumping technology. J. Proc. Mech. Eng 219(3) , (2005), 285–300.

8. S. Jiangzhou, R. Z. Wang, Y. Z. Lu, Y. X. Xu, and J. Y. Wu, Experimental investigations on adsorption air-conditioner used in internal-combustion locomotive driver-cabin. Applied Thermal Engineering 22(10), (2002), 1153–1162.

9. M. Tatlier, The effects of thermal and mass diffusivities on the performance of adsorption heat pumps employing zeolite synthesized on metal supports. Microporous and Mesoporous Materials 28(1), (1999), 195–203.

10. L. Marletta, A. Maggio, M. Freni, M. Ingrasciotta and G. Restuccia, A non-uniform pressure dynamic model of heat and mass transfer in compact adsorbent bed. Int. J. Heat and Mass Transfer 45(16), (2002), 3321–3320.

11. S. Waszkiewicz, S. Jenkins, H. Saidani-Scott and M. Tierney, Analysis of a finned heat exchanger working in an adsorption refrigeration system using zeolite and methanol. Heat Transfer Engineering 24(6), (2003), 71-78.

12. S. Prasertmanukitch, M. Tierney, S. Waszkiewicz, H. Saidani and I. Riceh, Measurement of the bulk adsorption properties of powders. Separation and Purification Technology 40(3), (2004), 267–277.

13. D. Tchernev, A waste heat driven automotive air conditioning system. Proc. Int. Sorption Heat Pump Conference, Munich, (1999) , 65-70.

14. R. Thorpe, Personal communication.

15. R.E.Critoph and S. J. Metcalf, Specific cooling power intensification limits in ammonia–carbon adsorption refrigeration systems. Applied Thermal Engineering 24(5), (2004), 661-678.

16. M. Tierney, H. Saidani-Scott, T. Eib and S. Prasertmerkitch, The purification of dilute CO2/ air solutions with an annular bed adsorber: numerical and experimental investigations. Separation and Purification Technology 17(2), (1999), 159–171.

17. B. A. Finlayson, The method of weighted residuals and variational principles, Academic Press, New York and London, 1972.

18. M. Al-Arabi and B. Sakr, Natural convection heat transfer from inclined isothermal plates. Int. J. Heat Mass Transfer 31(3), (1988), 559–566.

19. Wolverine Tube Inc.(Huntsville, US), Wolverine tube heat transfer data book, www.wlv.com/products/databook/databook.pdf (2001).

LIST OF FIGURES

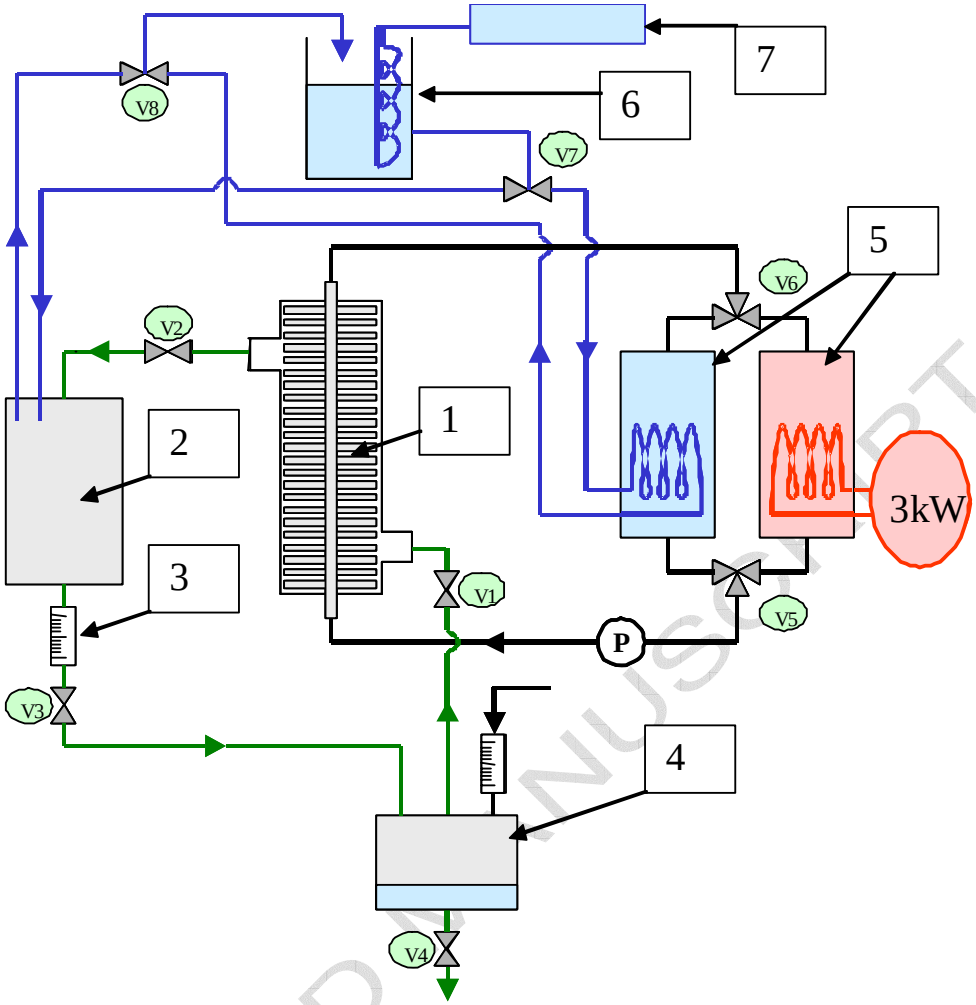

Fig. 1

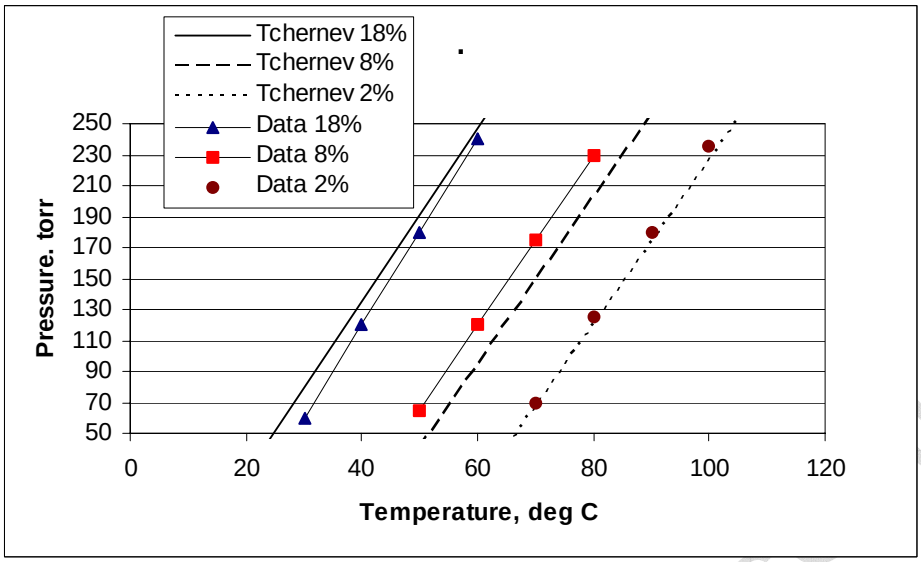

Part (a)

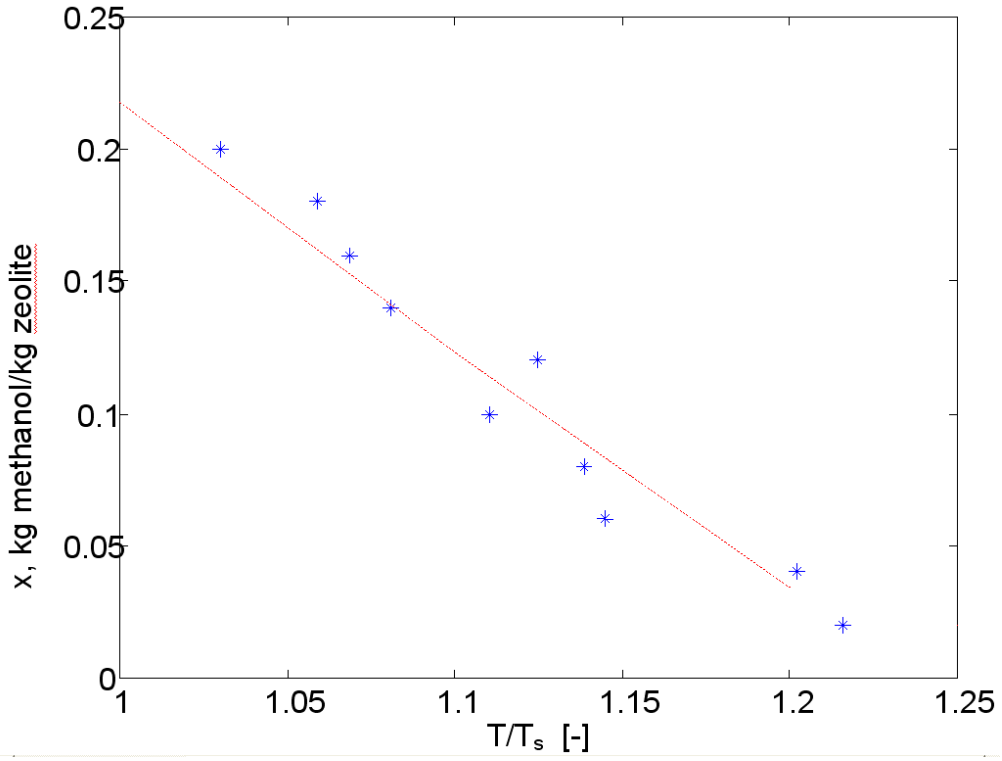

Part (b)

Fig. 2

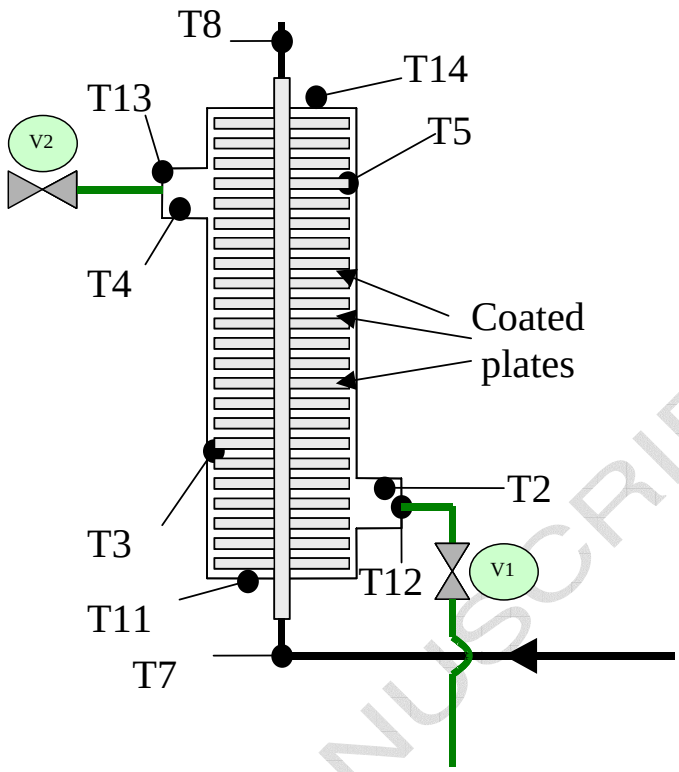

Fig. 3

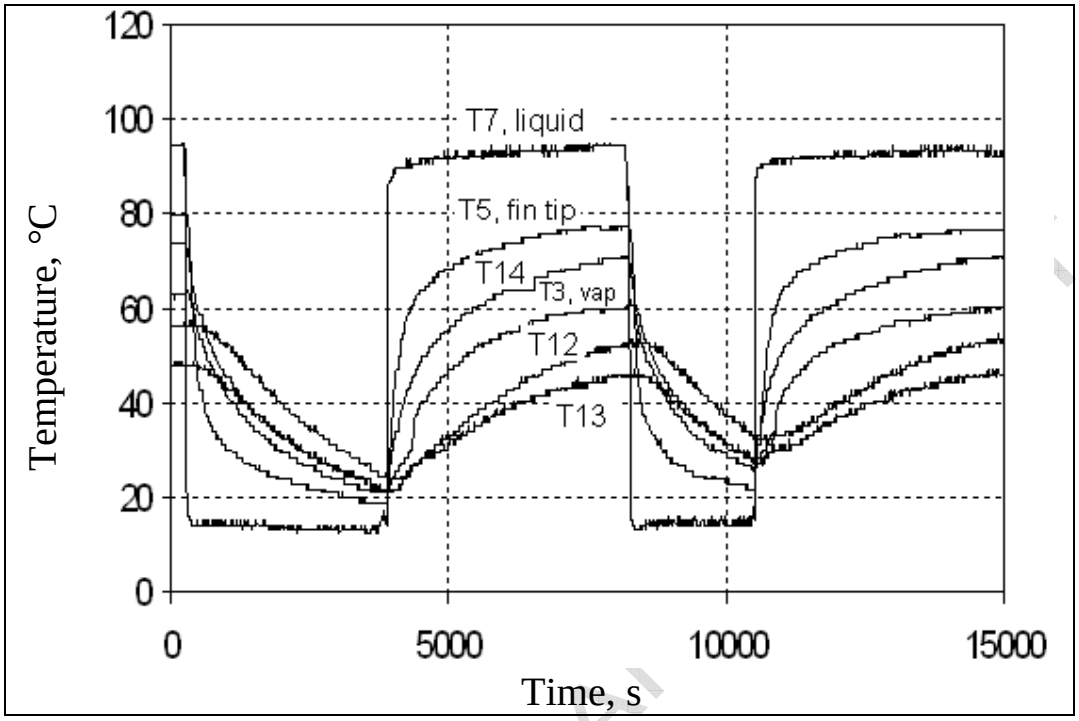

Fig. 4

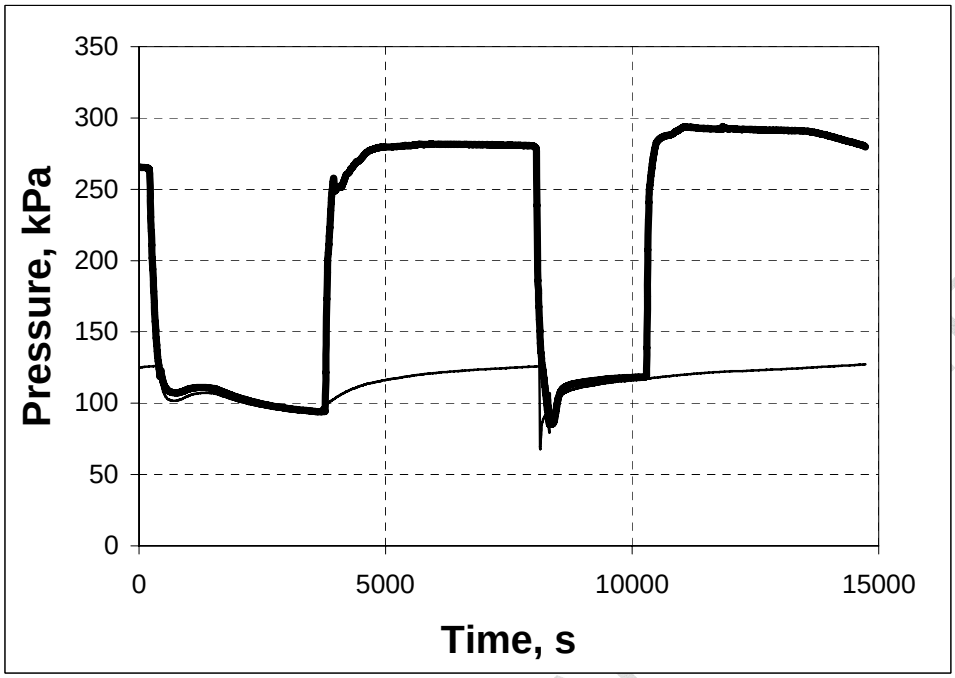

Fig 5

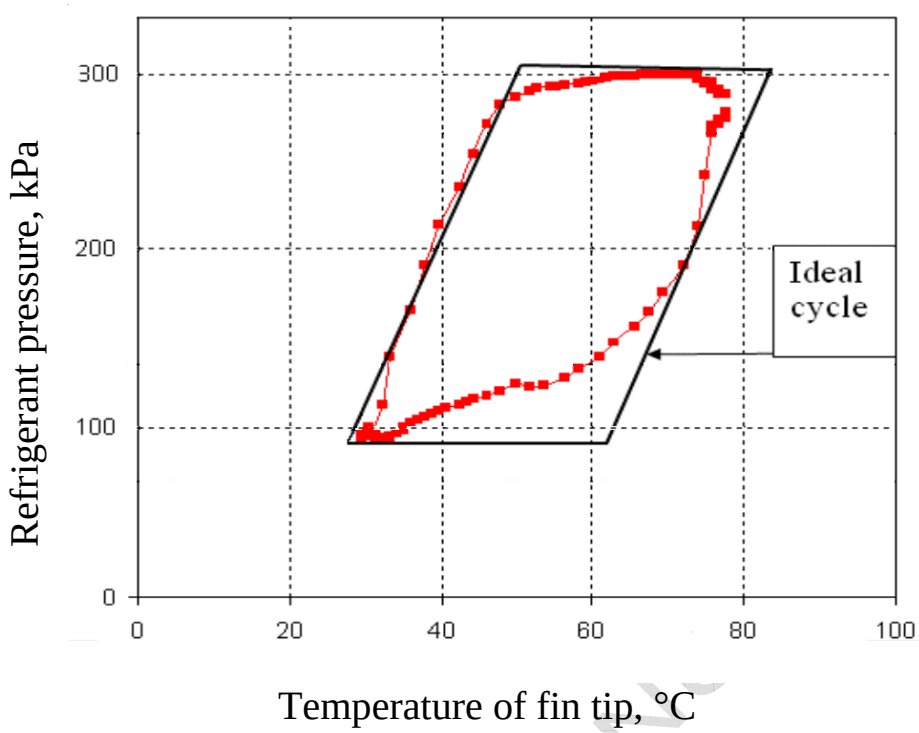

Fig. 6

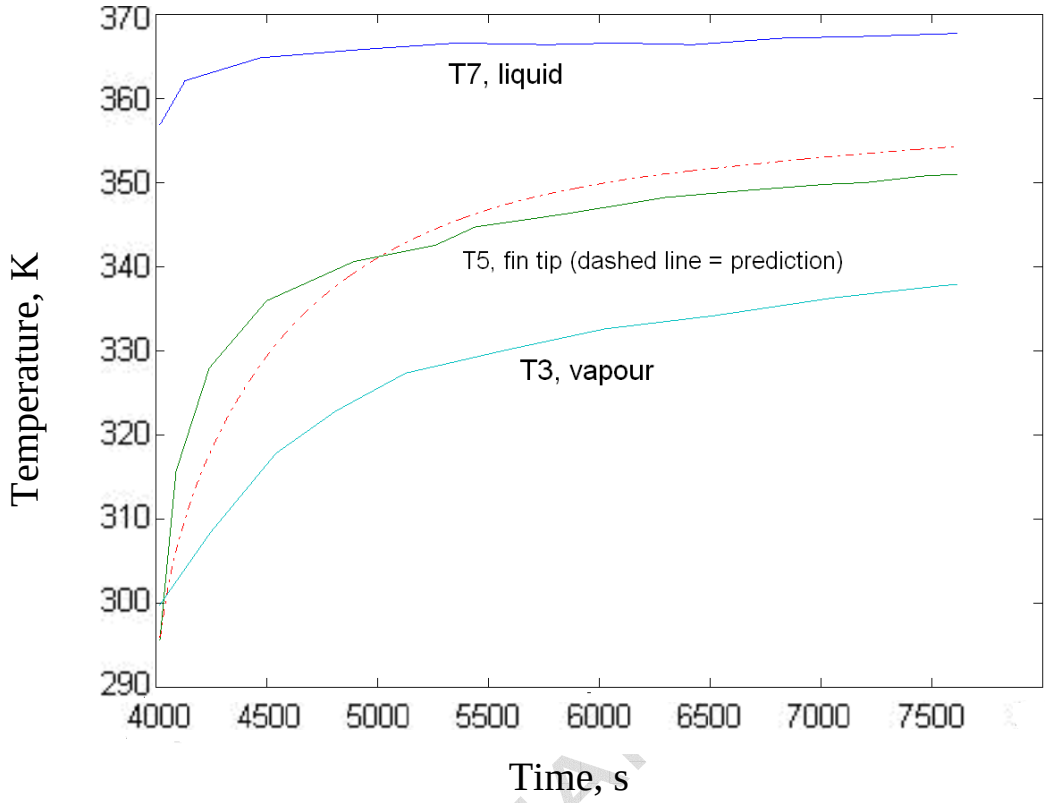

Fig. 7

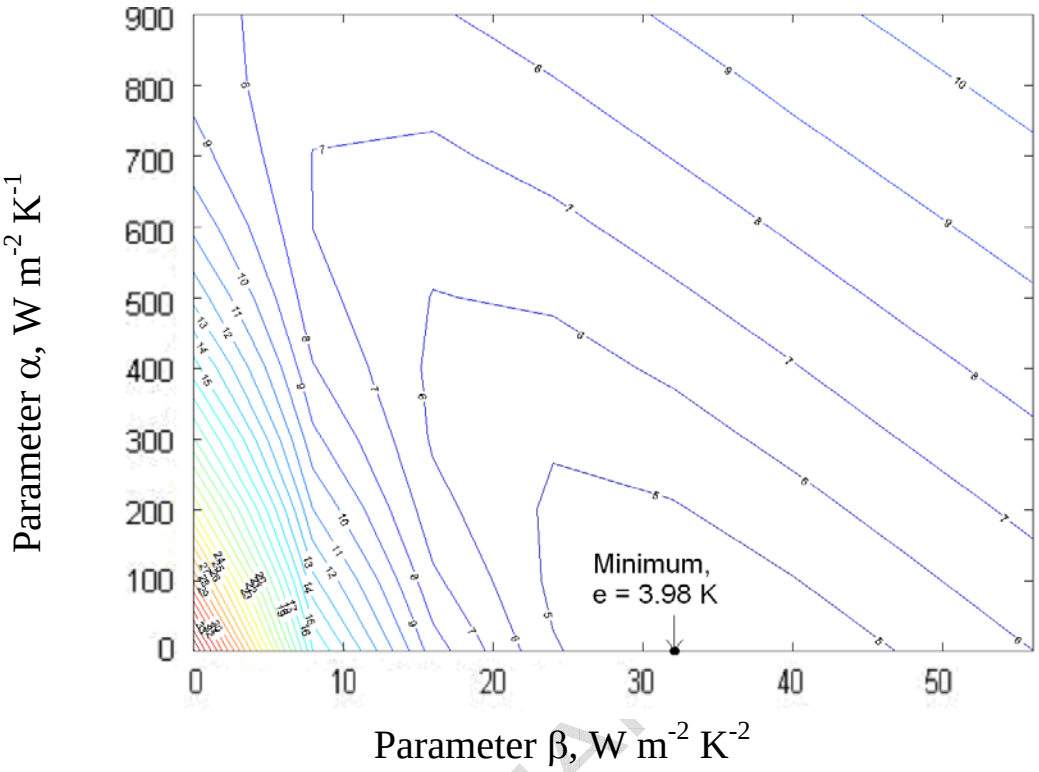

Fig 8.